Cardiomyopathy mutations in the tail of beta cardiac myosin modify the coiled-coil structure and affect integration into thick filaments in muscle sarcomeres in adult cardiomyocytes.

Marcin Wolny[1], Melanie Colegrave[1], Lucy Colman[1], Ed White[2], Peter J. Knight[1] and Michelle Peckham[1]

[1]From the School of Molecular and Cellular Biology, and [2]School of Biomedical Sciences and Multidisciplinary Cardiovascular Research Centre, Faculty of Biological Sciences, University of Leeds, Leeds, LS2 9JT, UK.

*Running title: *Effects of mutations in β-cardiac myosin tail*

To whom correspondence should be addressed: to Michelle Peckham, School of Molecular and Cellular Biology, Faculty of Biological Sciences, Miall Building, University of Leeds, Leeds, LS2 9JT, UK. Tel.: 0044 (0)113 343 4348; Fax.: 0044 (0)113 343 2835; Email: m.peckham@leeds.ac.uk

Key words: myosin, hypertrophic cardiomyopathy, coiled coil, structure, cardiomyocytes

Background: It is unclear how mutations in the coiled-coil tail of β-cardiac myosin cause heart disease.
Results: Effects of disease-causing mutations in the myosin tail were studied in vivo and in vitro.
Conclusion: Mutations that reduce helical content in vitro reduce sarcomere incorporation of myosin in vivo.
Significance: A change in myosin tail structure can lead to heart disease.

SUMMARY

It is unclear why mutations in the filament forming tail of myosin heavy chain (MHC) cause hypertrophic (HCM) or dilated (DCM) cardiomyopathy as these mutations should not directly affect contraction. To investigate this, we first investigated the impact of five HCM-causing (N1327K, E1356K, R1382W, E1555K and R1768K) and one DCM-causing (R1500W) tail mutations on their ability to incorporate into muscle sarcomeres in vivo. We used adenoviral delivery to express full-length wild type or mutant eGFP-MHC in isolated adult cardiomyocytes. Three mutations (N1327K, E1356K and E1555K) reduced eGFP-MHC incorporation into muscle sarcomeres while the remainder had no effect. No mutations significantly affected contraction. Fluorescence recovery after photobleaching (FRAP) showed that fluorescence recovery for the mutation that incorporated least well (N1327K), was significantly faster than that of WT with half times of 25.1 ± 1.8 and 32.2 ± 2.5 minutes (mean ± S.E.M.) respectively. Next, we determined the effects of each mutation on the helical properties of wild type and 7 mutant peptides (7, 11 or 15 heptads long) from the myosin tail by circular dichroism. R1382W and E1768K slightly increased the α-helical nature of peptides. The remaining mutations reduced α-helical content, with N1327K showing the greatest reduction. Only peptides containing residues 1301-1329 were highly α-helical suggesting that this region helps in initiation of coiled coil. These results suggest that small effects of mutations on helicity translate into a reduced ability to incorporate into sarcomeres, which may elicit compensatory hypertrophy.

β-cardiac myosin is a conventional class 2 myosin expressed in the heart and in slow muscle. It contains two heavy and four light chains. The heavy chains dimerise by forming a coiled-coil tail in the C-terminal region of the molecule and separate to form two globular heads at their N-terminal region. The globular head contains the motor domain, which binds actin and nucleotide and is responsible for generating contraction. The coiled-coil tail contains two α-helices that interact with each other to bury hydrophobic residues, forming a hydrophobic seam (1). Each contains a distinctive heptad repeat sequence in the form of $(abcdefg)_n$ where *a* and *d* are commonly hydrophobic. Because the heptad repeat is slightly

shorter than two turns of an α-helix, the two helices twist around each other to form a coiled coil with a left-handed superhelix (2). The tail also contains four "skip" residues, nominally at positions T1188, E1385, E1582 and G1807, which interrupt the heptad motif and correlate to bends in the myosin tail in the isolated molecules (3). The distal region of the coiled-coil tail assembles into thick filaments as a result of patterns of alternating charge along the length of the coiled coil (4), and a short assembly competence domain near the C-terminus (5).

Mutations in the gene for the heavy chain of β-cardiac myosin (MYH7) (6) cause the disease hypertrophic cardiomyopathy (HCM), a global disease that causes heart failure, first described over 50 years ago (7). HCM is the most common cause of sudden death in people under thirty years of age (8) and affects at least 1 in 500 people. Mutations in MYH7 cause approximately 40% of cases of inherited HCM (9,10). The disease is characterised by thickening of the left ventricular wall and myocardial disarray (11). More generally, mutations in genes that encode sarcomeric proteins are responsible for HCM (12) with over 630 mutations in 10 sarcomeric genes described as causing this disease. Mutations in MYH7 also cause dilated cardiomyopathy (DCM), a rarer heart disease that only affects about 1 in 2500 people (13), and characterised by a thinning of the ventricular walls (ventricular dilatation). Currently, over 200 HCM and 24 DCM mutations have been described for MYH7 (14), many of which result in a highly malignant form of the disease. However, tail mutations are rare and only limited descriptions of their severity and phenotype are available (Table S1).

While a clear link between HCM causing mutations in the motor domain and HCM can be attributed to direct effects on force output (11), it is unclear why mutations in the distal tail result in HCM. As the main role of the tail is to form filaments, it is unlikely that mutations in the tail directly affect force output. However, effects on coiled-coil structure and/or packing of the coiled coil into the thick filament, might affect myosin incorporation into thick filaments in sarcomeres, and thus indirectly affect force output over the longer term.

To test this idea, we investigated 5 different mutations that result in HCM (15-21) and one (R1500W) that causes dilated cardiomyopathy (DCM) (17). Only two of these mutations have been investigated previously (E1356K and R1500W (22,23)). In those reports, expressed and purified LMM peptides containing the mutation had decreased thermal stability, but the secondary structure was not affected. This suggested to us that any effects on secondary structure could be localised and not observable in the full-length LMM. Thus, in this study, we have used shorter peptides to investigate the effects of the mutations. Neither of these previous reports investigated the effects of these mutations *in vivo*.

Here, we have investigated the effects of each of these mutations on the incorporation of full-length β-cardiac myosin heavy chain, fused to eGFP (eGFP-MHC), *in vivo*. We used an adenoviral expression system to express eGFP-MHC in adult rat cardiomyocytes, and determined whether these mutations affect incorporation of the full-length heavy chain into the sarcomere or contraction. To determine if the effects we observed were correlated to effects on peptide structure *in vitro*, we analysed the secondary structure and thermal stability of peptides of different length. We used peptides that were 7, 11 or 15 heptads long from the myosin coiled-coil tail to determine if any or all of the 5 different mutations affect molecular structure, and to determine if the effects observed depended on peptide length.

EXPERIMENTAL PROCEDURES

Expression and characterisation of eGFP-MHC in adult cardiomyocytes - The full-length cDNA for the heavy chain of MYH7 (24) was cloned into an adenoviral expression vector (pdc315, Adgene) with eGFP fused to the N-terminus to generate eGFP-MHC. A second construct, without eGFP was also constructed. Purified virus (at MOIs between 50 and 100) was used to infect isolated adult rat cardiomyocytes. These were prepared from isolated rat hearts using a Langendorff retrograde perfusion technique with a collagenase containing solution (25). After incubation for 24 hours at 37°C, to allow the MHC to be expressed, cells were fixed using 4% formaldehyde in phosphate buffered saline prior to staining for other proteins of interest. Cells were stained with antibodies against an M-line epitope of titin (Ti51; kind gift of Dieter Furst (26)), or for

myosin heavy chain (A4.1025 antibody(27)), and cells were imaged using a Deltavision deconvolution microscope.

Levels of eGFP-MHC expression were compared to endogenous levels of MHC by SDS gel analysis using a protocol that separates MHC isoforms in a minigel system (28). Briefly, the separating gel contained 35% v/v glycerol, 9%w/v acrylamide-Bis (49:1), 230mM Tris HCl, 115 mM glycine, pH 8.8 and 0.4% w/v SDS; and the stacking gel contained 47% v/v glycerol, 6% w/v acrylamide-Bis (49:1), 110 mM Tris HCl, 6 mM EDTA, pH 6.8 and 0.4% w/v SDS). Gels were stained, or proteins were transferred to nitrocellulose paper to perform western blotting, using an antibody to MHC (A4.1025) or to eGFP (Abcam). These blots confirmed which band was endogenous and which the eGFP-tagged myosin in the stained gel (Fig. 1).

As expression levels were ~10% or less after 24 hours, we also attempted to culture MHC expressing cardiomyocytes for longer time periods. However, we found that long-term culture of cardiomyocytes resulted in a loss of contractility of the intact cells and in a loss of the characteristic rod-shape, as previously documented (29). We also suspect that the large excess of the overexpressed MHC compared to other myosin-binding proteins (light chains, titin, MyBP-C, actin etc) that are also needed to incorporate and regulate the MHC into muscle sarcomeres contributed to the loss of contractility as large amounts of unregulated soluble non-incorporated MHC may be toxic to the cells. Thus 24 hours of myosin overexpression is the best compromise between expression of high enough levels of eGFP-MHC to observe the impacts of the mutants within the sarcomere and expression of such high levels that cell viability is lost.

Fluorescence Recovery after Photobleaching (FRAP) - For FRAP experiments, cells were plated onto laminin-coated glass bottomed dishes (35mm, Iwaki), infected with the adenovirus, cultured overnight and imaged the following day using an inverted Zeiss 510 confocal microscope. Dishes were placed onto the heated stage (set to 37˚C), 10-15 cells were selected, their positions marked, and a Zeiss multi-time series macro was programmed to image each cell in turn, bleach a small rectangular area in each cell, approximately 2 sarcomeres in width, using 20 cycles of maximum laser power (at a wavelength of 488nm), and then image each cell every 5-10 minutes after bleaching for the next 105-125 minutes at 1% laser power until fluorescence recovery reached a plateau. To analyse the data, the average intensity of the bleached area was measured at each time point using ImageJ. Recordings from cells that contracted, or underwent large movements during the experiment were discarded. The average image intensity of the same sized area in an area adjacent to that bleached was also measured, to test that the intensity of non-bleached regions did not change. Data were normalised as described (30). Exponential fits to the data were generated using Prism (Graphpad).

Cardiomyocyte contraction - Within 18-24 hours of infection, live cells were placed in a bath, continuously perfused with physiological saline at room temperature, and stimulated by external platinum electrodes at a frequency of 1Hz to investigate their ability to contract. Contraction was recorded using video edge detection (31), and analysed for the times to peak shortening and half relaxation together with contractility, indexed as the amplitude of shortening as a % of resting cell length.

Expression and characterisation of coiled-coil peptides - Standard PCR based cloning was used to generate expression vectors for GST fusion proteins, using the MYH7 cDNA as a template. All constructs were sequence verified after cloning. The resulting expression vectors were used to express peptides in *E. coli*. During purification, the GST was removed using Precission protease. All peptides (Table S2) contained the N-terminal sequence GPLGS in addition to the peptide sequence. Each peptide expressed was designed to start and end on a residue in the *d* position of the heptad repeat. Peptides were 55, 83 or 111 residues long (7, 11 or 15 heptads, respectively). The 7-heptad peptides were designed such that in mutants, the mutated residue was in the central heptad with 3 heptads on either side. The concentrations of the purified proteins were determined by a micro BCA assay (Pierce) and/or by measuring their absorbance at 280nm in a quartz cuvette on a Cary-50 spectrophotometer and using the extinction coefficient calculated from the sequence (using ProtParam (ExPASy)). 7-heptad peptides were

additionally analysed by mass spectrometry, to confirm that their molecular mass was correct.

Circular dichroism - Circular dichroism spectra were measured from 260 to 190 nm at 10˚C using a Jasco J715 spectropolarimeter.

For the 7H peptides, protein concentrations varied from 0.25 mg/ml to 0.05 mg/ml, and their CD spectra were obtained at 10˚C at pH 8.0 in 150 mM NaCl, 10 mM phosphate buffer. Thermal melt data were obtained either in the same buffer, or in 50 mM NaCl, 10 mM phosphate buffer, at pH 7.0. An increase in pH slightly increased the Tm (melting temperature) for all the peptides equally. 1 mM DTT was added to peptides containing a cysteine residue.

The effect of the mutations on α-helical content was estimated by comparing the value of the ellipticity measurements (θ_{222}) at a wavelength of 222nm, expressed as mean residue ellipticity in degrees cm^2 $dmol^{-1}$ for the peptides at 10˚C for all the constructs. The θ_{222} values indicate the relative helical content of the peptides. We therefore used θ_{222} values to compare helical content between the constructs. Repeat measurements for the majority of the 7H constructs gave consistent results, giving confidence that the observed differences between peptides are likely to be significant, especially where differences are large. Where more than 2 repeats were performed for the 7H constructs, error bars are shown in Figure 5. To compare helical contents between peptides, the 222nm value was divided by -36,000 (theoretical value for 100% helical content) (32)

For the 11H and 15H peptides, protein concentrations varied from 0.25 mg/ml to 0.1 mg/ml and their CD spectra were obtained at 10˚C in 50 mM NaCl, 10 mM phosphate buffer, pH 7.4. Further data obtained in the same buffer at pH 7.0 (not shown) showed very little change in the spectra at a temperature of 10˚C. Three repeat measurements were made for each of the 11 and 15H peptides, and t-tests used to determine if differences in helical content (estimated from the 222nm value as described above) were significant.

The effect of temperature on the α-helical content was measured by taking measurements at 222 nm from 5 to 60˚C, for every 1˚C temperature change. The conditions used were 50 mM NaCl, 10 mM phosphate buffer, at pH 7.0. Temperature was changed at a rate of 2˚C/min. The temperature was returned to 10˚C and the resulting spectrum was close to that measured prior to heating (value at 222 nm, to within a few per cent). The θ_{222} measurements were normalised, by setting the value at 5˚C to 0% unfolded, and the value at 65˚C to 100% unfolded. The resulting plots of the θ_{222} values were fit using the Boltzman sigmoidal fit function in Graph Pad Prism 6 software (33), to generate values for Tm.

RESULTS

Expression of full-length MHC in cardiomyocytes - WT eGFP-MHC was expressed successfully in isolated adult cardiomyocytes, and the eGFP-tagged MHC (in which eGFP is fused to the MHC N-terminus (motor domain)) incorporated into the thick filaments in muscle sarcomeres. eGFP-MHC began to be expressed and to incorporate into sarcomeres 6-7 hours after viral infection (Fig. S1). After 24 hours, the pattern of fluorescence for eGFP-MHC was similar to the immunostaining pattern for total MHC, using an antibody against an epitope in the motor domain (Fig. 1A).

Both the anti-MHC immunostaining and the eGFP fluorescence show two stripes, separated by an unstained gap, which corresponds to the bare zone in the centre of the thick filament. The unstained gap at the M-line was wider (~0.3μm) for eGFP-MHC than for endogenous myosin (Fig. 1B), suggesting that there is some limit on incorporation of new myosin in the centre of the thick filament, as reported earlier (34). The gap in intensity at the I-band is similar for eGFP-MHC and the immunostained image for MHC (Fig. 1B). Overall, the newly synthesised eGFP-MHC has incorporated generally throughout the thick filaments, and not only at the very edges of the A-bands or at the periphery of the myofibrils, similar to that reported for embryonic chicken MHC in embryonic cardiomyocytes (35), although the fluorescence intensity is higher at the ends of the A-band. This suggests that myosin may exchange more easily at the ends of the thick filaments, because of the reduced number of interactions that myosin there makes with other myosins, as the thick filament tapers at this point. It is also possible that diffusion is faster within the I-band (less congested) than with the A-band, so that exchanging molecules are more likely to encounter thick filament ends

Impact of tail mutations on MHC uptake into myofibrils - Using the adenoviral expression system, we expressed and characterised six different tail mutants (N1327K, E1356K, R1382W, R1500W, E1555K and E1768K) in adult cardiomyocytes. These mutations are all found in the tail of MHC (Table S2, Fig. 5A). WT and mutant eGFP-MHC were all expressed at a level of 5-10% of the endogenous myosin, following 24 hours infection with the adenovirus as shown by SDS-PAGE gel and western blotting (Fig. 1B), with the exception of R1500W, which was expressed at slightly lower levels (~2% of endogenous myosin).

Deconvolution microscopy of fixed cardiomyocytes containing expressed mutant eGFP-MHC isoforms showed that in the case of several mutants, eGFP-MHC did not incorporate into muscle sarcomeres as well as WT eGFP-MHC in substantial numbers of cells (Fig. 2). Instead, eGFP-MHC incorporation was limited to regions at the edges at the A-bands, where it is mainly incorporated into the ends of the thick filament, and there were increased numbers of filamentous aggregates outside the myofibrils (Fig. 2B). These filamentous aggregates are likely to contain eGFP-MHC that is unable to incorporate or exchange into the sarcomeric thick filaments. We repeated these experiments several times, and consistently observed this effect.

Quantifying the proportions of cells with normal, or limited incorporation showed that the mutation N1327K resulted in the highest increase in the proportion of cells with limited incorporation of eGFP-MHC and this increase was significant (Fig. 2B). Two further mutations, E1356K and E1555K, also showed a trend towards an increase in numbers of cells with limited eGFP MHC incorporation. In the remaining three mutations, R1500W, R138W and E1768K, eGFP MHC incorporation was similar to wild type. The differences in incorporation are unlikely to be due to different levels of viral infection, as similar MOIs were used in all the experiments, and the expression levels of the eGFP MHC are low and uncorrelated with these differences (Fig. 1B).

Exchange rate of MHC into myofibrils using FRAP - The expression of full length eGFP-MHC in living adult cardiomyocytes gave us the opportunity, for the first time, to investigate how quickly eGFP-MHC exchanges into thick filaments using FRAP for WT and mutant isoforms. For WT eGFP-MHC, the fluorescence recovery was slow, with a half time for recovery of 32.2 ± 2.5 minutes (mean ± S.E.M, n= 14) (Fig. 3B). Recovery appeared to occur first in regions close to the Z-discs (arrowed, Fig 3A), before spreading through the rest of the A-band. While the rate of recovery was slow, these experiments showed that the myosin molecules are exchanging into and out of the thick filament more dynamically than we might have predicted.

We extended these FRAP experiments to two different mutants, one that had the most effect on sarcomeric incorporation (N1327K) and one that had the least (R1382W). We found that the half time for fluorescence recovery was significantly faster ($p<0.05$) for N1327K ($t_{½}$ of 25.1 ± 1.8 minutes (n=18)), but not for R1382W ($t_{½}$ of 31.0 ± 1.6 minutes (n=18)) compared to WT eGFP-MHC (Fig. 3B). These results suggest that the poorer incorporation of the N1327K mutation is linked to an increase in the rate of exchange of the MHC into thick filaments. The rate of myosin exchange into the thick filaments is partly determined by the rate at which the incoming myosin incorporates, as well as the rate of myosin dissociation.

Contractile properties of transfected cardiomyocytes - We did not find any significant differences between the contractile properties of untransfected cardiomyocytes and those expressing untagged MHC, WT eGFP-MHC or mutant isoforms of eGFP-MHC (Fig. 4). This might be thought to be due to the low expression levels of the eGFP MHC in our experiments (5-10% of endogenous myosin). However, modelling has suggested that expressing α-cardiac MHC myosin at similar expression levels on a background of β-MHC has an observable effect on contraction kinetics (36). Therefore, if the mutations studied here were able to exert a strong effect on contraction, we would have observed it in these experiments. Including the eGFP tag did not affect contraction, with no significant difference between any of the parameters measured for cells expressing un-tagged MHC compared to eGFP-tagged MHC. Moreover, the contractile properties of myocytes expressing WT eGFP-MHC were not significantly different from untransfected cells. These results suggest that none of the tail mutations, expressed at up to 10% of the

endogenous level of myosin, directly affect contraction.

Helical propensity of WT tail peptides containing 7, 11 or 15 heptads - The reduced incorporation of mutant eGFP-MHC into thick filaments in muscle sarcomeres for 3 out of the 6 mutants could be due to alterations in the structure of the coiled-coil tail. To test this, we expressed and purified WT and mutant peptides containing 7, 11, or 15 heptad repeats from the region of coiled coil that contains these mutations (Fig. 5, Table S2).

We expected that all of the wild type (WT) peptides would be α-helical and form coiled coil. Unexpectedly, only 7H1, 11H1 and 15H1 WT peptides had a high α-helical content at 10˚C (Fig. 5, Table 1), with the helical content increasing with length from 57% for 7H1 to 91% for 15H1. The five remaining 7H peptides tested (7H2 – 7H6, Fig. 5A,C) as well as 11H2 and 15H2 (Fig. 5F) were all less than 30% α-helical. The low helical content of many peptides indicates that they are unlikely to spend most of their time as a dimer, and thus as a coiled coil.

The α-helical content of WT 11H1 and 15H1 peptides both showed the sigmoidal dependence on temperature expected for the co-operative melting of a coiled coil (Fig. 5G & H). The Tm was 27°C for 11H1 and increased to 30°C for 15H1 (Table 1). A melting curve obtained for WT 7H1 (at pH 7.0) was less sigmoidal in shape (Supplemental Fig. 2), and the estimated Tm was lower (17°C). The increasing Tm with increasing peptide length suggests that the longer peptides are more stable.

These results demonstrate that sequences within the distal myosin tail vary widely in their propensity to form α-helix. Among those that we tested, only those containing residues 1301-1330 had a high helical propensity (Fig. 5A). Plotting the sequence of this region as a heptad net (37) (Fig. 6) shows that there it contains a short leucine zipper surrounded by many oppositely charged residues that can interact to stabilise a helical conformation. This region of sequence is likely to have a high propensity to form a coiled coil, and may help longer helical peptides to do so, explaining the high helical nature of the 7, 11 and 15H1 peptides.

Impacts of mutations on helical content of tail peptides - The mutation that had the most severe effect on sarcomeric incorporation in vivo, N1327K, significantly decreased the α-helical content of 7H1, 11H1 and 15H1 peptides (Fig. 5 B-C, E-F). The size of this decrease became less marked as the length of the peptide increased (~27% decrease for 7H1, ~16% for 11H1 and ~11% for 15H1 (Fig. 5C & G, Table 1)). N1327K also reduced the Tm (Fig. 5D & H, Table 1), with the effect larger in the 11H1 than in the 15H1 peptide. This mutation could be tested in each of the different length peptides (7H1, 11H1 and 15H1) due to its position in the sequence. A second mutation (E1356K) that reduced sarcomeric incorporation *in vivo* significantly reduced the helical content of the 11H peptide (by 21%, Fig. 5E,G), but had no effect on the 15H peptide (Fig. 5F,G), or on Tm (Fig. 5D & H, Table 1).

A further mutation (R1382W) that did not affect sarcomere incorporation *in vivo* significantly increased the helical content of the 15H peptide (Fig. 5F,G). The Tm was also increased for the mutant 15H peptide (Fig. 5H and Table 1). This suggests that R1382W, close to the skip residue (E1385), increases α-helical stability.

The three remaining mutations tested were in regions of the coiled coil that did not appear to form highly helical structures as 7, 11 or 15H peptides. R1500W (in 7H3), and E1555K (in 7H4) both appeared to decrease helical content, and E1768K (in 7H5) was the only mutation in the 7H peptides that appeared to increase helical content. However, the helical contents of the wild type peptides are low and the differences are not significant.

Overall, these peptide data show that N1327K has the greatest effect on the α-helical nature of the myosin coiled coil, reducing α-helical content and stability, whereas R1382W appears to increase the α-helical content and stability of the coiled coil.

DISCUSSION

Our data suggest that a reduced incorporation of mutant MHC into muscle sarcomeres is correlated with a large effect on the helical content of isolated peptides. Two mutations (N1327K and E1356K) that reduced α-helical content of peptides in solution also caused a reduction in sarcomeric incorporation of eGFP-MHC *in vivo*. In contrast, R1382W increased the α-helical

content of a 15 heptad peptide in solution, but had little effect on the incorporation of WT eGFP-MHC into sarcomeres *in vivo*. Local disruptions to the helical nature of the rod portion of MHC may thus contribute to the underlying mechanism by which these mutations result in disease. None of the mutations appeared to have strong effects on contraction at the levels of expression (5-10% of endogenous myosin) obtained in our experiments, which is consistent with the progressive etiology of HCM. Finally, N1327K, the mutation that has the most effect on sarcomeric incorporation and α-helical content, showed a faster rate of exchange into thick filaments in FRAP experiments compared to WT and to R1382W eGFP-MHC.

A new trigger sequence in the myosin tail - Unexpectedly, as part of our research into the effects of mutations in vitro, we discovered that most 50 amino acid residue peptides do not form 100% coiled coil in isolation. We had expected that the α-helical conformation of the 7 heptad peptides would be rapidly stabilised by forming a coiled coil, as all of them show a hydrophobic seam in their sequence (Fig 6A-F). However, with the exception of 7H1, all the 7H peptides had a low α-helical content, suggesting that they remain largely unfolded and/or form an alternative fold. Moreover, increasing the lengths of such peptides to 11 or even 15 heptads did not necessarily increase the α-helical content. Peptides had to contain the sequence within residues 1301-1329 to contain significant amounts of α-helix/coiled coil, suggesting that this region is important for coiled coil formation, possibly acting as a 'trigger sequence' in the tail. Trigger sequences have a high propensity to form α-helix and then assemble to form coiled coil with the trigger sequence region on a second peptide (38). This promotes folding and coiled-coil formation along the whole molecule. Any sequence that favours interchain and intrachain interactions may act as a trigger (39).

Plotting the 7H1 as a heptad net (Fig 6A) shows that there are many potential attractive intrachain interactions (including Q-E interactions) between successive turns of helix within 1309-1322 (boxed region, Fig. 6A), which will promote formation of α-helix. These interactions surround a short leucine zipper (leucines in the *a*, *d* and subsequent *a* positions). Together, these may account for the stability and helix propensity of this region of the coiled coil. Fewer interactions, and a lack of leucine residues in the hydrophobic seam may explain why downstream sequences (7H2-6, 11H2 and 15H2) have a lower propensity to form coiled coil in isolation. However, when the sequences of 7H2 and 7H3 (Fig 6B,C), are incorporated into 11H1 and 15H1, they do become helical presumably due to the influence of the upstream sequence from 7H1.

Molecular basis of effects of tail mutations - All of the mutations we studied affected the helical content and coiled coil formation of 7H peptides. Three mutations, N1327K, E1356K and E1555K, which decreased helical content in isolated peptides, also decreased incorporation of full-length myosin into the thick filament *in vivo*. This suggests that reducing the helical content could contribute to a decreased ability of these mutant isoforms to incorporate normally into thick filaments, and an increased chance that the mutant myosin forms aggregates outside the muscle sarcomeres. This may explain why all three of these mutations result in a more severe form of HCM (18,20) (Table S1). The non-incorporated aggregated myosin may be proteotoxic, supporting the recently suggested idea that protein misfolding is a major contributor to hypertrophic cardiomyopathy (40).

The reduced helical content that we observed for each of these three mutations may result from the introduction of an intra-chain repulsion. N1327K (*b* position in the heptad) introduces an intra-chain repulsion between this residue and K1323 in the preceding turn of helix (Fig. 6A). E1356K replaces an intra-chain attraction between this residue and R1359 into a repulsive one (Fig. 6B), which is likely to affect coiled coil stability. In contrast, E1555K (*e* position) replaces a potentially repulsive interaction between this residue and E1552 with an attractive one (Fig. 6D). Finally, our observation that the effects of mutations on α-helical content decrease as the lengths of the peptide increase helps to explain why an earlier study, using the full-length filament-forming region of the tail (LMM), found no effect of E1356K on α-helical content (22).

In addition to reducing helical content, each of these mutants, in residues on the outside of the coiled coil, has the potential to affect packing of the myosin heavy chain into the thick filament. Both E1356 (in a '*c*' position) and E1555K ('*e*'

position) are in patches of glutamates (Fig. 6B & D). A mutation to lysine decreases the net charge of these patches by two. This has the potential to affect integration of the molecule into the thick filament, which depends on the pattern of alternating negative and positive charge along the coiled coil (41). In addition, E1555K is in a region of LMM implicated in binding to other thick filament proteins such as Myosin Binding Protein C (MyBPC; thought to lie between residues 1554 and 1581), Myomesin and M-protein (thought to lie between residues 1506 and 1674) (42-44). While mutation of E1555 to Q in earlier experiments showed it did not affect MyBPC binding (42), it has not been determined if E1555K affects binding of MyBPC, myomesin and/or M-line protein.

Two further mutations, R1382W and E1768K had little effect on sarcomeric incorporation but are associated with increased helical content in the 15H and 7H peptides respectively. R1382W (*a* position, Fig. 6F) is close to one of the skip residues (E1385), thought to correlate to the bends in the myosin tail in the extended molecule (3). This mutation may increase α-helical content by stabilising the sequence close to the skip residue, as tryptophan is more hydrophobic than arginine, and may become more buried (Fig 6F). In addition, this mutation would abolish any inter-chain attractive forces between R1382 (*a* position) and both D1378 and E1385 in adjacent *d* positions. E1768 (*g*) is partnered with Q1773 (e) on the other helix, which cannot form an ionic interaction (Fig 6E). However, within the chain it can make an ionic interaction with K1771. Its mutation to K would result in a repulsive interaction with K1771 (Fig. 6E), but introduce a novel ionic interchain bonding with E1772 (*d*) emerging from the coiled-coil seam. This might be expected to disfavour helix stability, in contrast to our observation that this mutation increases the helical content of a weakly helical 7H peptide. Thus the mechanism of disease by these apparently benign mutations remains obscure.

R1500W causes DCM rather than HCM, albeit with a late onset (age 55+ (17)). We found that this mutation abolished the already low helical content of a 7H peptide. R1500W could decrease α-helical content through the loss of a potential attractive force between R1500 (*f* position) and E1496 (*b*) (see Fig. 6C). This mutation also replaces a polar residue with a bulky hydrophobic one, in an 'f' position in the heptad repeat in which residues are usually polar. In the tail of wild type β-MHC, tryptophan is not found in any of the 'f' positions in the heptad repeats. Introducing a bulky hydrophobic residue out in solution as a result of this mutation might be expected to affect molecular structure. Previous work has shown that this mutation decreases the Tm of LMM (by 2.3°C) and decreases assembly into filaments *in vitro* (as observed by light scattering) (23). However, we found that this mutation had little effect on sarcomeric incorporation in vivo.

Exchange of myosin in thick filaments is quicker than turnover - The rate of exchange of eGFP MHC into myofibrils that we observed in FRAP experiments is much faster than the slow rate of turnover of MHC protein in the beating heart. The half-life for myosin turnover is long, recently measured as ~15 days in hearts from rats (45). Similarly, exchange rates for several Z-disc proteins measured using FRAP were also found to be much faster than the turnover rates for these proteins (46). A rapid exchange rate would enable newly synthesised MHC to be rapidly and efficiently exchanged into the thick filament within the muscle sarcomere, without disassembling the existing myofibrils, thus maintaining force output.

Our experiments with N1327K showed that this mutation increased exchange rates. We think it is likely that the other mutations in the rod domain of myosin that result in HCM could also affect exchange rates. This change in exchange rates could result from the reduction in local helical stability. This suggests the possibility that in patients harbouring mutations in the myosin rod, disease results from a defective exchange/turnover process, which has the potential to decrease force output in the heart. Interestingly, this has some analogies with skeletal muscle diseases such as Laing distal myopathy, a disease of skeletal muscle that also involves mutations in the rod portion of myosin, and results in muscle weakness (47). Defective myosin is known to accumulate outside the muscle sarcomeres in this disease. It is also possible that the mutation also affects the 6S-10S equilibrium, although it is unknown whether cardiac muscle myosin adopts a compact conformation in vivo. A partially compact conformer has been observed in vitro (48).

We have reported here, for the first time, that eGFP MHC can incorporate normally into muscle sarcomeres, without affecting contraction, and that eGFP-MHC can exchange into muscle sarcomeres, (half time of about 30 minutes). This is the first time that the behaviour of a full-length eGFP-MHC has been studied in adult cardiomyocytes and that it has been directly demonstrated the myosin can exchange into thick filaments. Since the thick filament contains 294 myosin molecules (49), the measured FRAP half time suggests a molecule of myosin exchanges into a thick filament every 10 seconds on average, making the thick filament a more dynamic assembly than is generally perceived.

Our approach of expressing eGFP-tagged full-length MHC in adult rat cardiomyocytes using an adenoviral delivery system has allowed us to measure the dynamic behaviour of myosin in live cells as well as to directly investigate the impact of HCM mutations *in vivo*. By contrast, previous studies have used a GFP-tagged myosin tail (50,51), or untagged MHC (52), or expressed the eGFP-MHC in neonatal rather than adult cardiomyocytes (53). This methodology should have wide applicability to gaining understanding of the mechanism of cardiomyopathies deriving from any myofibrillar protein.

References

1. Parry, D. A., Fraser, R. D., and Squire, J. M. (2008) Fifty years of coiled-coils and alpha-helical bundles: a close relationship between sequence and structure. *J Struct Biol* **163**, 258-269
2. Offer, G., and Sessions, R. (1995) Computer modelling of the alpha-helical coiled coil: packing of side-chains in the inner core. *J Mol Biol* **249**, 967-987
3. Offer, G. (1990) Skip residues correlate with bends in the myosin tail. *J Mol Biol* **216**, 213-218
4. Atkinson, S. J., and Stewart, M. (1992) Molecular interactions in myosin assembly. Role of the 28-residue charge repeat in the rod. *J Mol Biol* **226**, 7-13
5. Cohen, C., and Parry, D. A. (1998) A conserved C-terminal assembly region in paramyosin and myosin rods. *J Struct Biol* **122**, 180-187
6. Geisterfer-Lowrance, A. A., Kass, S., Tanigawa, G., Vosberg, H. P., McKenna, W., Seidman, C. E., and Seidman, J. G. (1990) A molecular basis for familial hypertrophic cardiomyopathy: a beta cardiac myosin heavy chain gene missense mutation. *Cell* **62**, 999-1006
7. Maron, B. J., Seidman, C. E., Ackerman, M. J., Towbin, J. A., Maron, M. S., Ommen, S. R., Nishimura, R. A., and Gersh, B. J. (2009) How should hypertrophic cardiomyopathy be classified?: What's in a name? Dilemmas in nomenclature characterizing hypertrophic cardiomyopathy and left ventricular hypertrophy. *Circ Cardiovasc Genet* **2**, 81-85; discussion 86
8. Maron, B. J., Chaitman, B. R., Ackerman, M. J., Bayes de Luna, A., Corrado, D., Crosson, J. E., Deal, B. J., Driscoll, D. J., Estes, N. A., 3rd, Araujo, C. G., Liang, D. H., Mitten, M. J., Myerburg, R. J., Pelliccia, A., Thompson, P. D., Towbin, J. A., and Van Camp, S. P. (2004) Recommendations for physical activity and recreational sports participation for young patients with genetic cardiovascular diseases. *Circulation* **109**, 2807-2816
9. Maron, B. J. (2009) The 2009 international hypertrophic cardiomyopathy summit. *Am J Cardiol* **105**, 1164-1168
10. McNally, E. M. (2002) Beta-myosin heavy chain gene mutations in familial hypertrophic cardiomyopathy: the usual suspect? *Circ Res* **90**, 246-247
11. Ho, C. Y. (2012) Hypertrophic cardiomyopathy in 2012. *Circulation* **125**, 1432-1438
12. Maron, B. J. (2002) Hypertrophic cardiomyopathy: a systematic review. *JAMA* **287**, 1308-1320
13. Taylor, M. R., Carniel, E., and Mestroni, L. (2006) Cardiomyopathy, familial dilated. *Orphanet J Rare Dis* **1**, 27
14. Xu, Q., Dewey, S., Nguyen, S., and Gomes, A. V. (2010) Malignant and benign mutations in familial cardiomyopathies: insights into mutations linked to complex cardiovascular phenotypes. *J. Mol. Cell. Cardiol.* **48**, 899-909
15. Blair, E., Redwood, C., de Jesus Oliveira, M., Moolman-Smook, J. C., Brink, P., Corfield, V. A., Ostman-Smith, I., and Watkins, H. (2002) Mutations of the light meromyosin domain of the beta-myosin heavy chain rod in hypertrophic cardiomyopathy. *Circ Res* **90**, 263-269
16. Hougs, L., Havndrup, O., Bundgaard, H., Kober, L., Vuust, J., Larsen, L. A., Christiansen, M., and Andersen, P. S. (2005) One third of Danish hypertrophic cardiomyopathy patients with MYH7 mutations have mutations [corrected] in MYH7 rod region. *Eur J Hum Genet* **13**, 161-165
17. Karkkainen, S., Helio, T., Jaaskelainen, P., Miettinen, R., Tuomainen, P., Ylitalo, K., Kaartinen, M., Reissell, E., Toivonen, L., Nieminen, M. S., Kuusisto, J., Laakso, M., and Peuhkurinen, K. (2004) Two novel mutations in the beta-myosin heavy chain gene associated with dilated cardiomyopathy. *Eur J Heart Fail* **6**, 861-868
18. Perrot, A., Schmidt-Traub, H., Hoffmann, B., Prager, M., Bit-Avragim, N., Rudenko, R. I., Usupbaeva, D. A., Kabaeva, Z., Imanov, B., Mirrakhimov, M. M., Dietz, R., Wycisk, A., Tendera, M., Gessner, R., and Osterziel, K. J. (2005) Prevalence of cardiac beta-myosin heavy chain gene mutations in patients with hypertrophic cardiomyopathy. *J Mol Med* **83**, 468-477
19. Richard, P., Charron, P., Carrier, L., Ledeuil, C., Cheav, T., Pichereau, C., Benaiche, A., Isnard, R., Dubourg, O., Burban, M., Gueffet, J. P., Millaire, A., Desnos, M., Schwartz, K., Hainque, B.,

and Komajda, M. (2003) Hypertrophic cardiomyopathy: distribution of disease genes, spectrum of mutations, and implications for a molecular diagnosis strategy. *Circulation* **107**, 2227-2232

20. Van Driest, S. L., Jaeger, M. A., Ommen, S. R., Will, M. L., Gersh, B. J., Tajik, A. J., and Ackerman, M. J. (2004) Comprehensive analysis of the beta-myosin heavy chain gene in 389 unrelated patients with hypertrophic cardiomyopathy. *J Am Coll Cardiol* **44**, 602-610
21. Waldmuller, S., Freund, P., Mauch, S., Toder, R., and Vosberg, H. P. (2002) Low-density DNA microarrays are versatile tools to screen for known mutations in hypertrophic cardiomyopathy. *Hum Mutat* **19**, 560-569
22. Armel, T. Z., and Leinwand, L. A. (2010) A mutation in the beta-myosin rod associated with hypertrophic cardiomyopathy has an unexpected molecular phenotype. *Biochem. Biophys. Res. Com.* **391**, 352-356
23. Armel, T. Z., and Leinwand, L. A. (2010) Mutations at the same amino acid in myosin that cause either skeletal or cardiac myopathy have distinct molecular phenotypes. *J. Mol. Cell. Cardiol.* **48**, 1007-1013
24. Miller, G., Maycock, J., White, E., Peckham, M., and Calaghan, S. (2003) Heterologous expression of wild-type and mutant beta-cardiac myosin changes the contractile kinetics of cultured mouse myotubes. *J. Physiol.* **548**, 167-174
25. McCrossan, Z. A., Billeter, R., and White, E. (2004) Transmural changes in size, contractile and electrical properties of SHR left ventricular myocytes during compensated hypertrophy. *Cardiovas. Res.* **63**, 283-292
26. Van der Ven, P. F., Ehler, E., Perriard, J. C., and Furst, D. O. (1999) Thick filament assembly occurs after the formation of a cytoskeletal scaffold. *J. Muscle Res. Cell Motil.* **20**, 569-579
27. Maggs, A. M., Taylor-Harris, P., Peckham, M., and Hughes, S. M. (2000) Evidence for differential post-translational modifications of slow myosin heavy chain during murine skeletal muscle development. *J. Muscle Res. Cell Motil.* **21**, 101-113
28. Picard, B., Barboiron, C., Chadeyron, D., and Jurie, C. (2011) Protocol for high-resolution electrophoresis separation of myosin heavy chain isoforms in bovine skeletal muscle. *Electrophoresis* **32**, 1804-1806
29. Leach, R. N., Desai, J. C., and Orchard, C. H. (2005) Effect of cytoskeleton disruptors on L-type Ca channel distribution in rat ventricular myocytes. *Cell calcium* **38**, 515-526
30. Snapp, E. L., Altan, N., and Lippincott-Schwartz, J. (2003) Measuring protein mobility by photobleaching GFP chimeras in living cells. *Current protocols in cell biology Edited by Juan S. Bonifacino [et al.]* **Chapter 21**, Unit 21
31. Miller, G., Maycock, J., White, E., Peckham, M., and Calaghan, S. (2003) Heterologous expression of wild-type and mutant beta-cardiac myosin changes the contractile kinetics of cultured mouse myotubes. *J Physiol* **548**, 167-174
32. Greenfield, N., and Fasman, G. D. (1969) Computed circular dichroism spectra for the evaluation of protein conformation. *Biochemistry* **8**, 4108-4116
33. Greenfield, N. J. (2006) Using circular dichroism collected as a function of temperature to determine the thermodynamics of protein unfolding and binding interactions. *Nat Protoc* **1**, 2527-2535
34. Wenderoth, M. P., and Eisenberg, B. R. (1987) Incorporation of nascent myosin heavy chains into thick filaments of cardiac myocytes in thyroid-treated rabbits. *J. Cell. Biol.* **105**, 2771-2780
35. Wang, Q., Moncman, C. L., and Winkelmann, D. A. (2003) Mutations in the motor domain modulate myosin activity and myofibril organization. *J. Cell. Sci.* **116**, 4227-4238
36. Locher, M. R., Razumova, M. V., Stelzer, J. E., Norman, H. S., and Moss, R. L. (2011) Effects of low-level alpha-myosin heavy chain expression on contractile kinetics in porcine myocardium. *Am. J. Physiol.* **300**, H869-878
37. Baboolal, T. G., Sakamoto, T., Forgacs, E., White, H. D., Jackson, S. M., Takagi, Y., Farrow, R. E., Molloy, J. E., Knight, P. J., Sellers, J. R., and Peckham, M. (2009) The SAH domain extends the functional length of the myosin lever. *Proc. Natl. Acad. Sci. (USA)* **106**, 22193-22198

38. Steinmetz, M. O., Jelesarov, I., Matousek, W. M., Honnappa, S., Jahnke, W., Missimer, J. H., Frank, S., Alexandrescu, A. T., and Kammerer, R. A. (2007) Molecular basis of coiled-coil formation. *Proc Natl Acad Sci U S A* **104**, 7062-7067
39. Lee, D. L., Lavigne, P., and Hodges, R. S. (2001) Are trigger sequences essential in the folding of two-stranded alpha-helical coiled-coils? *J. Mol. Biol.* **306**, 539-553
40. Willis, M. S., and Patterson, C. (2013) Proteotoxicity and cardiac dysfunction--Alzheimer's disease of the heart? *New Engl. J. Med.* **368**, 455-464
41. McLachlan, A. D., and Karn, J. (1982) Periodic charge distributions in the myosin rod amino acid sequence match cross-bridge spacings in muscle. *Nature* **299**, 226-231
42. Flashman, E., Watkins, H., and Redwood, C. (2007) Localization of the binding site of the C-terminal domain of cardiac myosin-binding protein-C on the myosin rod. *Biochem. J.* **401**, 97-102
43. Obermann, W. M., Gautel, M., Weber, K., and Furst, D. O. (1997) Molecular structure of the sarcomeric M band: mapping of titin and myosin binding domains in myomesin and the identification of a potential regulatory phosphorylation site in myomesin. *EMBO J.* **16**, 211-220
44. Obermann, W. M., van der Ven, P. F., Steiner, F., Weber, K., and Furst, D. O. (1998) Mapping of a myosin-binding domain and a regulatory phosphorylation site in M-protein, a structural protein of the sarcomeric M band. *Mol. Biol. Cell.* **9**, 829-840
45. Papageorgopoulos, C., Caldwell, K., Schweingrubber, H., Neese, R. A., Shackleton, C. H., and Hellerstein, M. (2002) Measuring synthesis rates of muscle creatine kinase and myosin with stable isotopes and mass spectrometry. *Anal. Biochem.* **309**, 1-10
46. Sanger, J. W., Wang, J., Holloway, B., Du, A., and Sanger, J. M. (2009) Myofibrillogenesis in skeletal muscle cells in zebrafish. *Cell Motil. Cytoskel.* **66**, 556-566
47. Meredith, C., Herrmann, R., Parry, C., Liyanage, K., Dye, D. E., Durling, H. J., Duff, R. M., Beckman, K., de Visser, M., van der Graaff, M. M., Hedera, P., Fink, J. K., Petty, E. M., Lamont, P., Fabian, V., Bridges, L., Voit, T., Mastaglia, F. L., and Laing, N. G. (2004) Mutations in the slow skeletal muscle fiber myosin heavy chain gene (MYH7) cause laing early-onset distal myopathy (MPD1). *Am. J. Hum. Gen.* **75**, 703-708
48. Jung, H. S., Komatsu, S., Ikebe, M., and Craig, R. (2008) Head-head and head-tail interaction: a general mechanism for switching off myosin II activity in cells. *Mol Biol Cell* **19**, 3234-3242
49. Craig, R., and Offer, G. (1976) Axial arrangement of crossbridges in thick filaments of vertebrate skeletal muscle. *J. Mol. Biol.* **102**, 325-332
50. Buvoli, M., Buvoli, A., and Leinwand, L. A. (2012) Effects of pathogenic proline mutations on myosin assembly. *J. Mol. Biol.* **415**, 807-818
51. Vandenboom, R., Herron, T., Favre, E., Albayya, F. P., and Metzger, J. M. (2011) Gene transfer, expression, and sarcomeric incorporation of a headless myosin molecule in cardiac myocytes: evidence for a reserve in myofilament motor function. *Am. J. Physiol.* **300**, H574-582
52. Herron, T. J., Vandenboom, R., Fomicheva, E., Mundada, L., Edwards, T., and Metzger, J. M. (2007) Calcium-independent negative inotropy by beta-myosin heavy chain gene transfer in cardiac myocytes. *Circ. Res.* **100**, 1182-1190
53. Becker, K. D., Gottshall, K. R., Hickey, R., Perriard, J. C., and Chien, K. R. (1997) Point mutations in human beta cardiac myosin heavy chain have differential effects on sarcomeric structure and assembly: an ATP binding site change disrupts both thick and thin filaments, whereas hypertrophic cardiomyopathy mutations display normal assembly. *J. Cell Biol.* **137**, 131-140
54. Peckham, M., and Knight, P. J. (2009) When a predicted coiled coil is really a single alpha-helix, in myosins and other proteins. *Soft Matter* **5**, 2493-2503

FOOTNOTES:

*This work was funded by a British Heart Foundation grant (PG/07/061/23277), a BBSRC funded studentship to LC and a BBSRC grant (BB/I007423/1) to MP, PJK and MW.

[1] To whom correspondence should be addressed: to Michelle Peckham, School of Molecular and Cellular Biology, Faculty of Biological Sciences, Miall Building, University of Leeds, Leeds, LS2 9JT, UK. Tel.: 0044 (0)113 343 4348; Fax.: 0044 (0)113 343 2835; Email: m.peckham@leeds.ac.uk

[2]Lucy Colman's current address is: The MRC Clinical Sciences Centre, Imperial College London.

3. The abbreviations used are: HCM, hypertrophic cardiomyopathy (HCM); MHC, Myosin heavy chain; WT, Wild type; FRAP, Fluorescence recovery after photobleaching

FIGURE LEGENDS

FIGURE 1. Expression and incorporation of eGFP-MHC in adult cardiomyocytes. **A**. The fluorescence pattern for eGFP-MHC 24 hours after adding adenovirus is similar to that observed for endogenous MHC, using an antibody that recognises the motor domain of myosin (A4.1025). Co-labelling with an anti-M-line titin antibody (Ti51) confirms that the wider gap in fluorescence observed for eGFP-MHC is at the M-line. Black arrows indicate the positions of Z-discs. B. Fluorescence images of part of a cardiomyocyte, corresponding to one myofibril in width, expressing eGFP-MHC and co-stained for MHC using an antibody. The corresponding line profiles for the fluorescence images are shown below, demonstrating how fluorescence intensity varies along the myofibril for MHC and for eGFP-MHC. Arrows indicate the positions of Z-discs. **C**. Images of a Coomassie stained SDS gel, and corresponding immunoblots probed using antibodies to eGFP or to myosin heavy chain (A4.1025) to identify the bands for eGFP-tagged and endogenous MHC.

FIGURE 2. Analysis of eGFP-MHC incorporation in adult cardiomyocytes. A. Representative images showing normal incorporation contrasted with poor incorporation with filamentous aggregates. Black arrows show the positions of Z-disks. White arrows show filamentous aggregates. The images shown are for the N1327K mutant. B. Quantification of eGFP incorporation for WT and each of the mutants. The results shown are the mean values (+/- SEM) for 3-6 experiments. The % of cells with aggregates (shown in white) was significantly higher in N1327K expressing cells compared to WT cells ($p<0.05$). The % of cells without aggregates is shown in grey.

FIGURE 3. FRAP analysis of eGFP-MHC dynamics in living cardiomyocytes. A: sample images from a FRAP experiment showing a region from a single cardiomyocyte expressing wild type eGFP-MHC, in which the bleached square is in the centre. The pre-bleach image, followed by the immediate post-bleach image, and subsequent images at 45 and 125 minutes are shown. Arrows indicate location of fluorescence recovery near Z-discs. B: Time course of FRAP data for WT (n=14), N1327K (n=18) and R1382W (n=18), showing the means +/- S.E.M. at each time point, and the exponential fits to the data.

FIGURE 4. Contraction data for rat ventricular myocytes cultured for 24 hours that were untransfected, expressing WT-MHC, WT GFP-MHC or mutant WT GFP-MHC. Myocytes were stimulated to contract at a frequency of 1Hz. Data are shown as mean ± S.E.M. Values for n are: 9 (Control Untransfected), 14 (WT MHC), 14 (WT GFP-MHC), 12 (N1327K) 20 (E1356K), 11 (R1382W), 14 (R1500W), 11 (E1555K) and 13 (R1768K). **A.** Time from stimulation to peak shortening. **B.** Time of half relaxation from peak shortening to resting cell length. **C.** Contractility expressed as the amplitude of cell shortening as a % of resting cell length. No significant differences were found between any of the measurements.

FIGURE 5. Properties of wild type and mutant peptides. **A.** Diagram of the positions of the tail peptides and mutants investigated in the tail. The black line represents a scale bar of 100 amino acids alongside the coiled-coil tail of the myosin. The positions of the 4 skip residues are shown by grey dotted lines. The shaded rectangles show the positions, with respect to their positions in the tail of myosin, of each of the peptides investigated, in which overlapping sequence in different peptides is shown in the same colour/pattern. E.g. heptad H1 is shown in black, and the start of heptad 7H2 is shown as black, as it contains the C-terminal sequence of heptad 7H1. The filled stars denote the relative α-helical content of each peptide (see key). The vertical rectangle shown using a dashed line shows the region of the sequence required for high α-helical content. B. CD spectra for the 7H1 WT and mutant (N1327K) peptides. (pH 8.0, 150mM NaCl, 10mM phosphate buffer) **C**. Summary plot of the values for θ_{222} (MRW) (which reports on α-helical content) measured for each of the WT 7H peptides (shown as black bars) and the corresponding mutant (shown as white bars). Conditions used were pH 8.0, 150mM NaCl, 10mM phosphate buffer. The mean together with the standard error is shown. The decrease in helical content for N1327K is significant ($p<0.05$). **D**. Normalised thermal melt curves for 11H peptides (pH 7.0, 50mM

NaCl, 10mM phosphate buffer). **E**. CD spectra for the WT and mutant 11H1 peptides (pH 7.4, 50mM NaCl, 10mM phosphate buffer). **F**. CD spectra for the WT and mutant 15H1 peptides (pH7.4, 50mM NaCl, 10mM phosphate buffer). **G**. Summary plot of the θ_{222} (MRW) values for the WT 11H1 (black bars), and 15H1 (black bars), mutant 11H1 and 15H1 peptides (white bars) as shown in **E** and **F**, together with the value for the WT 11H2 and 15H2 peptides (grey bars). Significant changes in helical content between WT and mutant peptides are indicated by asterisks, where * is $p<0.05$, ** is $p<0.01$ and *** is $p<0.001$. **H** Normalised thermal melt curves for 15H peptides (pH 7.0, 50mM NaCl, 10mM phosphate buffer).

FIGURE 6. Heptad net plots of each of the WT 7H peptides tested. A to F shows peptides 7H1 to 7H6. In each plot, the preferred intra-chain ionic interactions (see (37,54)) are shown as solid lines. In addition alternative/other interactions are shown as dotted lines. Every seventh residue is repeated on the right of the plot (in brackets) so that all interactions can be shown. The gray dashed lines indicate the path of the polypeptide backbone; the green dotted line defines the orientation of the α-helix axis. The light gray circles indicate ‘‘*a*’’ positions and the squares indicate ‘‘*d*’’ positions that form the hydrophobic seam. In A: the boxed region (dashed lines) within this 7H1 peptide that favours coiled coil formation is shown. The black hexagons (dashed lines) indicate the positions of the mutant residues within each sequence.

Table 1. Estimates of the % helical contents and melting temperatures (Tm) for each 11H and 15H peptide and associated mutant. Melting curves were only performed once. Tm was estimated as described in the methods.

Peptide	Mutation/WT	α-helical content (pH 7.4) (%) ± SEM	Tm pH 7.0 (10°C)	ΔTm compared to WT
11H1	WT	79 ± 1	26.9	-
11H1	N1327K	66 ± 2	22.3	-4.6
11H1	E1356K	62 ± 2	26.2	-0.7
15H1	WT	91 ± 1	29.7	-
15H1	N1327K	81 ± 3	27.8	-1.9
15H1	E1356K	90 ± 2	30.0	+0.3
15H1	R1382W	98 ± 2	33.8	+4.1

Figure 1

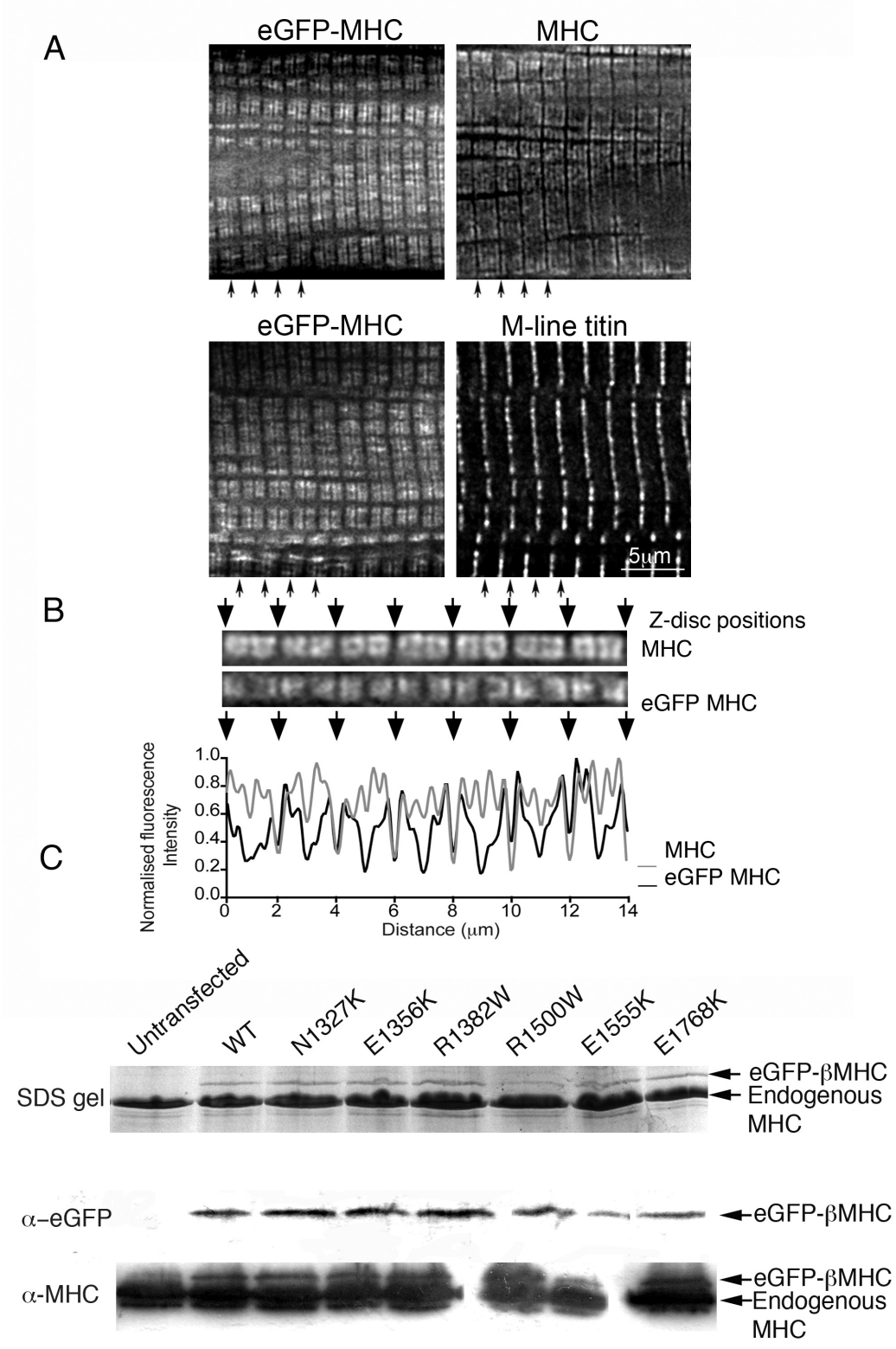
A
eGFP-MHC
MHC
eGFP-MHC
M-line titin
5μm
B
Z-disc positions
MHC
eGFP MHC
C
Normalised fluorescence Intensity
1.0
0.8
0.6
0.4
0.2
0.0
0
2
4
6
8
10
12
14
Distance (μm)
MHC
eGFP MHC
Untransfected
WT
N1327K
E1356K
R1382W
R1500W
E1555K
E1768K
SDS gel
eGFP-βMHC
Endogenous MHC
α–eGFP
eGFP-βMHC
α-MHC
eGFP-βMHC
Endogenous MHC

Figure 2

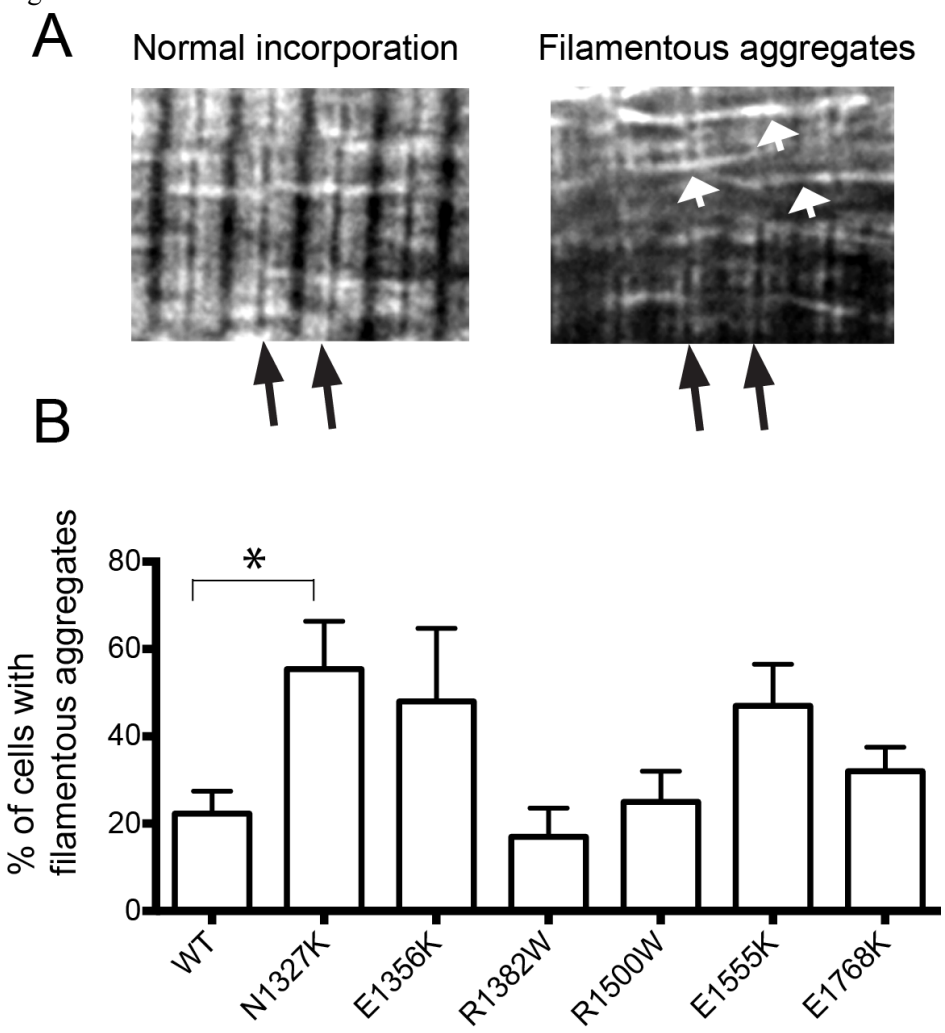
A
Normal incorporation
Filamentous aggregates
B
% of cells with filamentous aggregates
80
60
40
20
0
*
WT
N1327K
E1356K
R1382W
R1500W
E1555K
E1768K

Figure 3

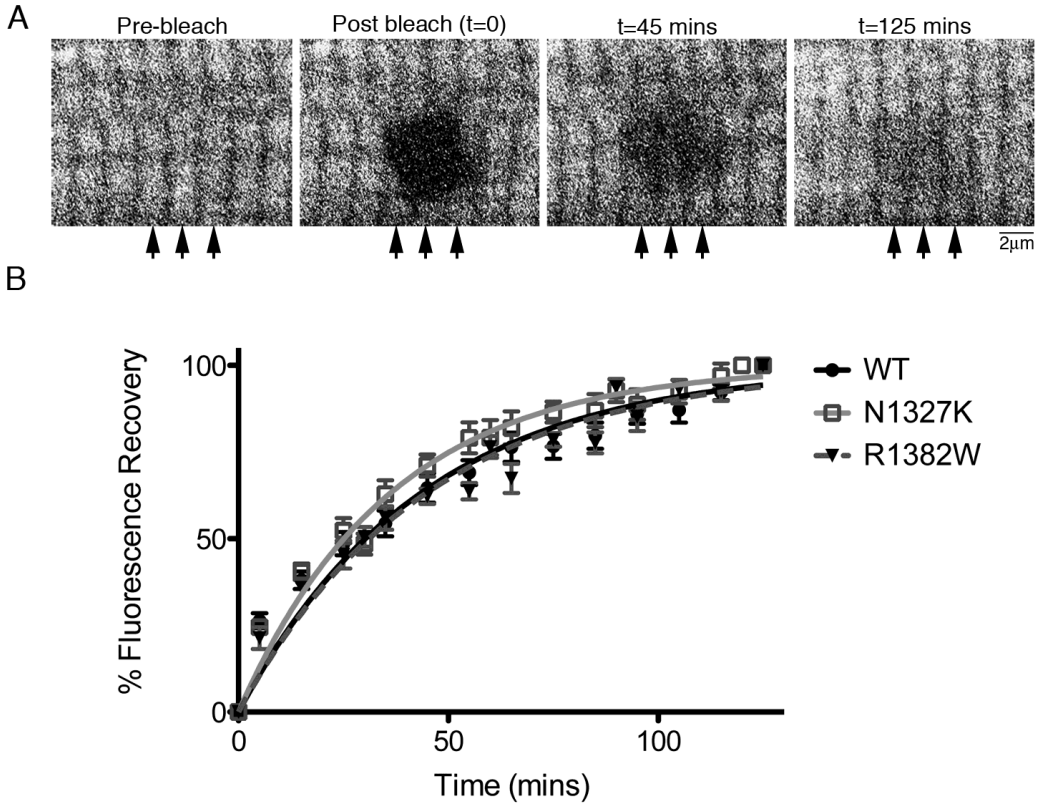
A
Pre-bleach
Post bleach (t=0)
t=45 mins
t=125 mins
2µm
B
% Fluorescence Recovery
100
50
0
0
50
100
Time (mins)
WT
N1327K
R1382W

Figure 4

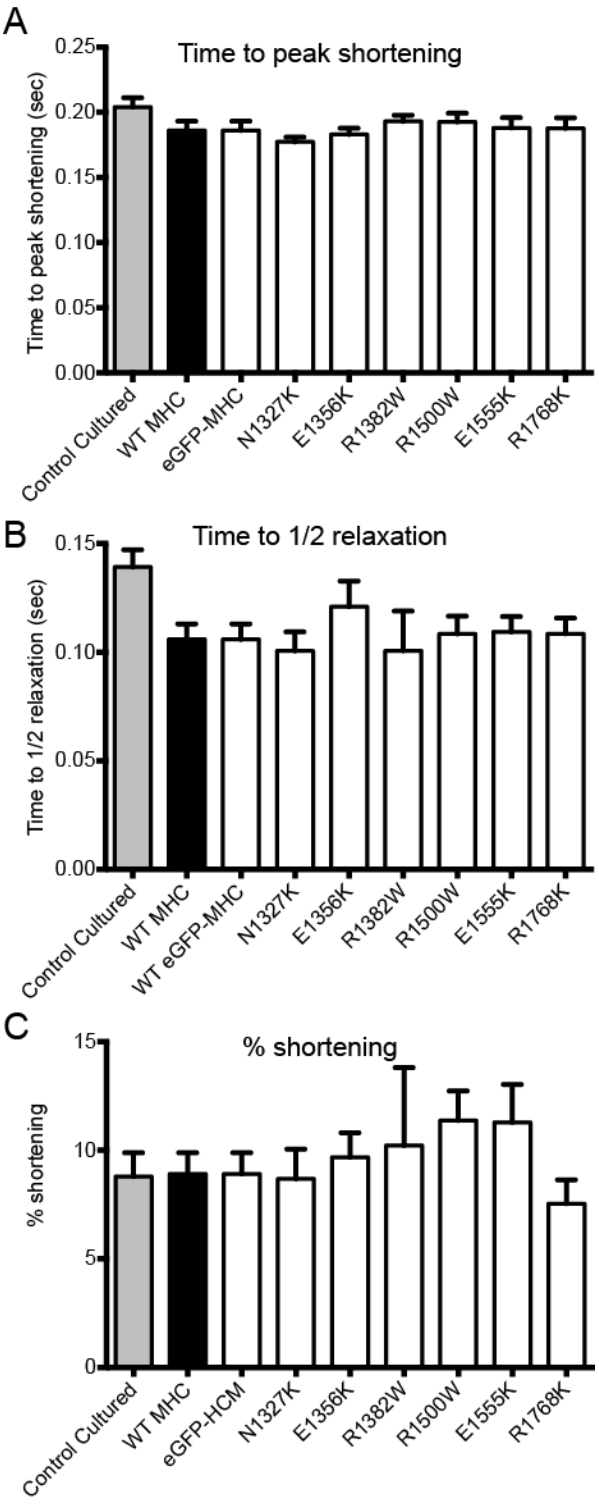
A
Time to peak shortening
Time to peak shortening (sec)
0.25
0.20
0.15
0.10
0.05
0.00
Control Cultured
WT MHC
eGFP-MHC
N1327K
E1356K
R1382W
R1500W
E1555K
R1768K
B
Time to 1/2 relaxation
Time to 1/2 relaxation (sec)
0.15
0.10
0.05
0.00
Control Cultured
WT MHC
WT eGFP-MHC
N1327K
E1356K
R1382W
R1500W
E1555K
R1768K
C
% shortening
% shortening
15
10
5
0
Control Cultured
WT MHC
eGFP-HCM
N1327K
E1356K
R1382W
R1500W
E1555K
R1768K

Figure 5

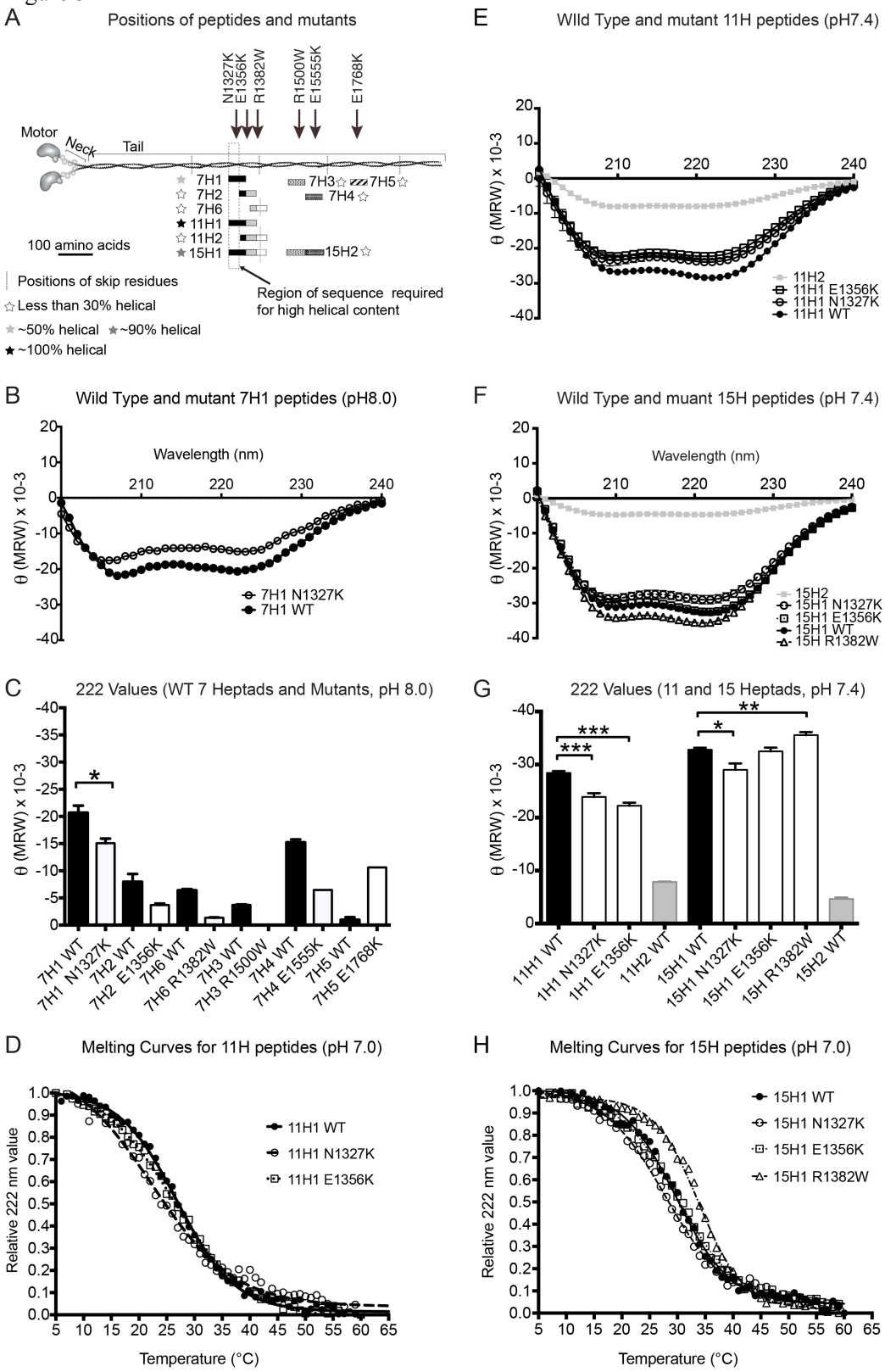
A
Positions of peptides and mutants
N1327K
E1356K
R1382W
R1500W
E15555K
E1768K
Motor
Neck
Tail
7H1
7H2
7H6
11H1
11H2
15H1
7H3
7H5
7H4
15H2
100 amino acids
Positions of skip residues
Less than 30% helical
~50% helical
~90% helical
~100% helical
Region of sequence required for high helical content
B
Wild Type and mutant 7H1 peptides (pH8.0)
Wavelength (nm)
θ (MRW) x 10-3
7H1 N1327K
7H1 WT
C
222 Values (WT 7 Heptads and Mutants, pH 8.0)
θ (MRW) x 10-3
7H1 WT
7H1 N1327K
7H2 WT
7H2 E1356K
7H6 WT
7H6 R1382W
7H3 WT
7H3 R1500W
7H4 WT
7H4 E1555K
7H5 WT
7H5 E1768K
D
Melting Curves for 11H peptides (pH 7.0)
Relative 222 nm value
Temperature (°C)
11H1 WT
11H1 N1327K
11H1 E1356K
E
WIld Type and mutant 11H peptides (pH7.4)
θ (MRW) x 10-3
11H2
11H1 E1356K
11H1 N1327K
11H1 WT
F
Wild Type and muant 15H peptides (pH 7.4)
Wavelength (nm)
θ (MRW) x 10-3
15H2
15H1 N1327K
15H1 E1356K
15H1 WT
15H R1382W
G
222 Values (11 and 15 Heptads, pH 7.4)
θ (MRW) x 10-3
11H1 WT
11H1 N1327K
11H1 E1356K
11H2 WT
15H1 WT
15H1 N1327K
15H1 E1356K
15H R1382W
15H2 WT
H
Melting Curves for 15H peptides (pH 7.0)
Relative 222 nm value
Temperature (°C)
15H1 WT
15H1 N1327K
15H1 E1356K
15H1 R1382W

Figure 6

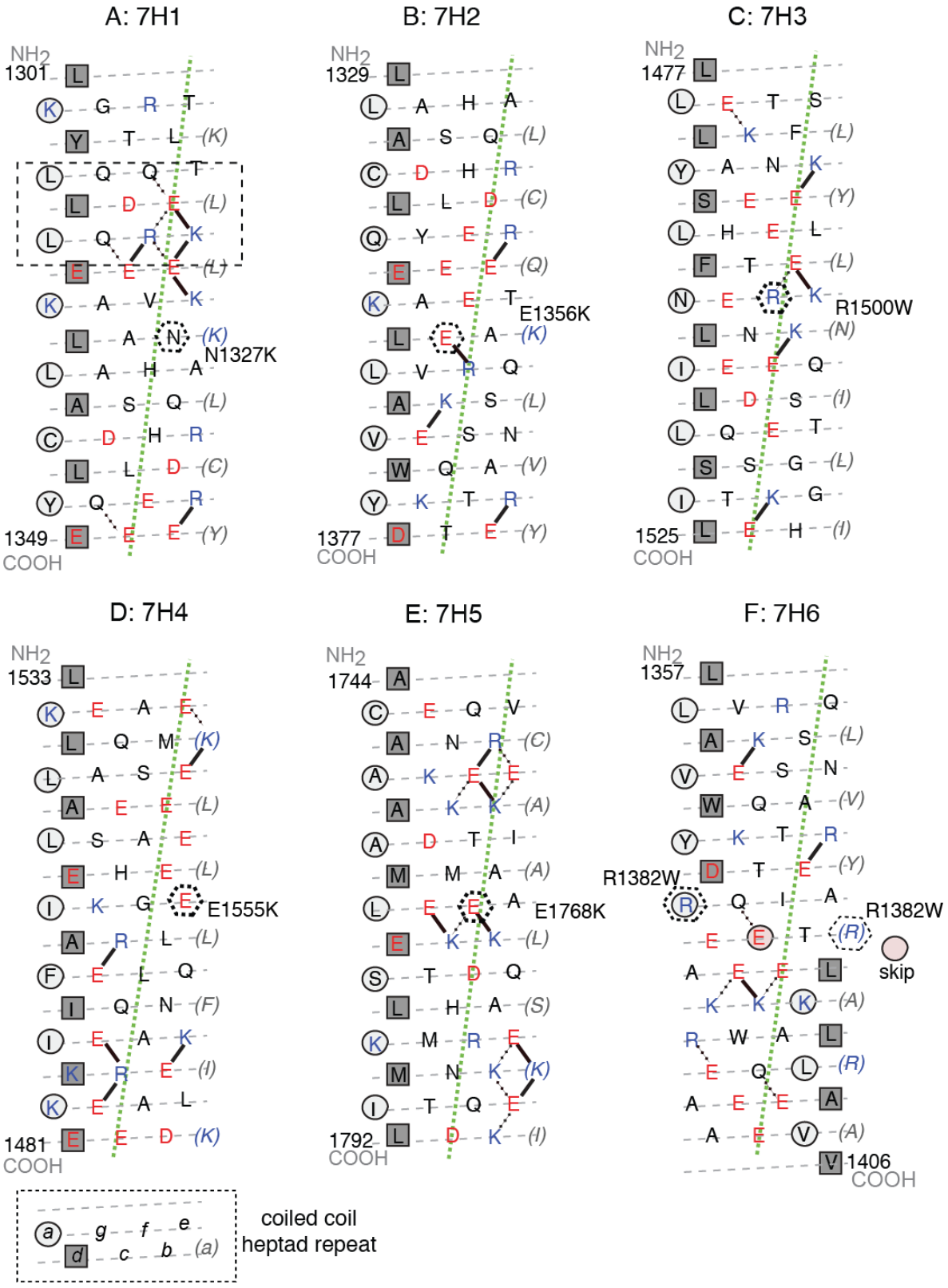
A: 7H1
B: 7H2
C: 7H3
D: 7H4
E: 7H5
F: 7H6
NH2
COOH
1301
1329
1477
1533
1744
1357
1349
1377
1525
1481
1792
1406
N1327K
E1356K
R1500W
E1555K
E1768K
R1382W
skip
coiled coil
heptad repeat